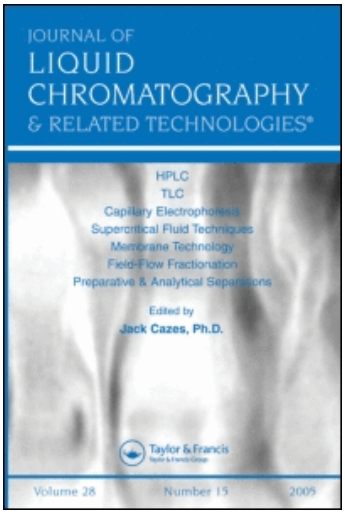


## Journal of Liquid Chromatography & Related Technologies

Publication details, including instructions for authors and subscription information:
http://www.informaworld.com/smpp/title~content=t713597273

# Feasibility Studies on Photophoretic Effects in Field-Flow Fractionation of Particles

V. L. Kononenko[a]; J. K. Shimkus[a]; J. C. Giddings[b]; M. N. Myers[b]
[a] Institute of Biochemical Physics Russian Academy of Sciences, Moscow, Kosygin, Russia [b] FFF Research Center The University of Utah, Salt Lake City, Utah, USA

**To cite this Article** Kononenko, V. L. , Shimkus, J. K. , Giddings, J. C. and Myers, M. N.(1997) 'Feasibility Studies on Photophoretic Effects in Field-Flow Fractionation of Particles', Journal of Liquid Chromatography & Related Technologies, 20: 16, 2907 — 2929
**To link to this Article: DOI:** 10.1080/10826079708005600
**URL:** http://dx.doi.org/10.1080/10826079708005600

J. LIQ. CHROM. & REL. TECHNOL., 20(16 & 17), 2907–2929 (1997)

# FEASIBILITY STUDIES ON PHOTOPHORETIC EFFECTS IN FIELD-FLOW FRACTIONATION OF PARTICLES

V. L. Kononenko,[1] J. K. Shimkus,[1,*] J. C. Giddings,[2] M. N. Myers[2]

[1] Institute of Biochemical Physics
Russian Academy of Sciences
117977 Moscow, Kosygin Street 4, Russia

[2] FFF Research Center
The University of Utah
Salt Lake City, Utah 84112, USA



## ABSTRACT

Various mechanisms of particles photophoresis, both of direct and indirect type, are considered theoretically. The analytical expressions are obtained for photophoretic and photo-thermophoretic mobilities of particles, and their dependence on particle size, optical, and physicochemical properties is analyzed. The motion of latex spheres, glass beads, and carbon black particles of 3-22 μm diameter, in water, under the action of focused $Ar^+$-ion laser beam, was studied experimentally at $\lambda$=514.5 nm and power 0.1-0.8 W, using two arrangements. In the first one, the particles' motion was observed through the microscope. The positive photophoresis (away from the light source) was registered for all kinds of particles. Photophoretic velocities of particles were evaluated in connection with their size, optical properties, and laser power density.

In another arrangement, the laser power was focused at the entrance glass window of a round metallic capillary, along its axis, in the direction of suspension flow inside the capillary. The elution curves for polydisperse carbon black particles were registered in the gravity-sedimentation FFF mode with the laser power switched on and off. Typical curves possessed a strong initial maximum, attributed to the fraction of smaller particles, and a substantially lower secondary maximum related to large particles. The action of light changed the shape of the first maximum and shifted to a smaller time the second one. Both experimental and theoretical results show the possibility to generate, under FFF conditions, the photophoretic velocities of particles in the range 1-100 mm/sec, depending on the light intensity, which are sufficient to accomplish their separation relative to size, optical, and surface charge properties.



## INTRODUCTION

The use of photophoresis, i.e., the motion of particles and molecules under the action of light, offers, potentially, many advantageous separation possibilities due to a great variety of particular mechanisms of light interaction with these objects.[1] However, the practical realization of Photophoretic FFF requires, apart from the solution of very specific technical problems, a more detailed investigation of the nature and manifestation conditions of various photophoretic mechanisms, as well as their connection to the size, optical, and relevant physicochemical properties of particles.

## MECHANISMS OF DIRECT PHOTOPHORESIS

There are two principal mechanisms of direct photophoresis. The first one, usually referred to as the *light pressure*, is associated with the momentum transfer from electromagnetic field to particles and molecules irradiated due to the scattering and absorption of light. The second one, named the *gradient force*, manifests itself in spatially inhomogeneous fields only, and has the same nature as the forces acting on electric or magnetic dipoles in static inhomogeneous electric or magnetic fields.

The calculations of both light pressure and gradient force are based on the solution of the light scattering problem for a particle of given shape and optical parameters. The latter are described by the complex refractive index of the particle material, relative to that of surrounding medium at the wavelength $\lambda$ of

light: $m(\lambda)=n_r(\lambda)-i\cdot\kappa(\lambda)$, $n_r$ being the relative refraction index, $\kappa$ being the index of absorption. In general, the final results can be obtained only numerically. However, the analytical results exist in some limiting cases, namely, for Rayleigh scattering, Rayleigh-Gans scattering, and for the case of very large particles.[2-6] Following the treatment reported in Ref. 6, let us consider a spherical particle of radius a placed in a wide, slightly divergent light beam with effective radius $w_0 >> a$ and angular divergence $|\Delta\theta| << 1$, $|\Delta\theta| \geq a/w_0$.

A particle is characterized by the size parameter $\rho=2\pi a/\lambda$. (There is a large diversity of notations used for the size parameter: x in Refs. 2, 4, 5, $\alpha$ in Refs. 3, 11, $\rho$ in Refs. 6-8, 14, and q in Ref. 15. We adopt $\rho$ here, keeping x for the coordinate notation in the optical problem).

It is assumed that relative complex dielectric permittivity $\varepsilon=\varepsilon'-i\cdot\varepsilon''$ and relative magnetic permeability $\mu=\mu'-i\cdot\mu''$ of particle material (related to the permittivity $\varepsilon_m$ and permeability $\mu_m$ of surrounding medium) satisfy the Rayleigh-Gans conditions $|\varepsilon-1|<<1$, $2\rho|\varepsilon-1| <<1$, $|\mu-1|<<1$, $2\rho|\mu-1| <<1$. (Note, that $\varepsilon'=n_r^2-\kappa^2$ and $\varepsilon''=2\, n_r\kappa$).

Then, the direct photophoretic force $F_{ph}$ can be written as a sum of the radiation-pressure force and the gradient force:[6]

$$\vec{F}_{ph} = \vec{F}_{pr} + \vec{F}_{\nabla} \ ,$$

$$\vec{F}_{pr} = \varepsilon_m \frac{\pi a^2}{c} Q_{pr}(\rho)\cdot\vec{J}_0 \ , \qquad (1)$$

$$\vec{F}_{\nabla} = \varepsilon_m \frac{2\pi a^3}{c}\left(\frac{\varepsilon'-1}{\varepsilon'+2}+\frac{\mu'-1}{\mu'+2}\right)\cdot\nabla\vec{J}_0 \ .$$

Here, $J_0$ is the incident light irradiance, measured in units of energy per unit time per unit area, c is the light velocity. The factor $Q_{pr}$ in Equation 1 is the dimensionless efficiency factor of radiation pressure, $Q_{pr}= Q_{ext}-\langle\cos\theta\rangle Q_{sca}$, and $Q_{ext}= Q_{sca}+ Q_{abs}$. Here $Q_{ext}$, $Q_{sca}$ and $Q_{abs}$ are the efficiency factors of the extinction, scattering, and absorption of light, $\langle\cos\theta\rangle$ is the cosine of the scattering angle $\theta$ weighted by the scattering diagram of a particle.[2-4]

It is convenient to introduce the transport efficiency factor $Q_{tr}=(1-\langle\cos\theta\rangle)Q_{sca}$, which describes the contribution to the light pressure from the light scattering only. In the case considered, these factors can be shown to be:

$$
\begin{aligned}
&Q_{pr}(\rho) = Q_{tr}(\rho) + Q_{abs}(\rho) \ , \\
&Q_{tr}(\rho) = \frac{9}{4}\left(\left|\frac{\varepsilon-1}{\varepsilon+2}\right|^2 + \left|\frac{\mu-1}{\mu+2}\right|^2\right)\cdot I_1(\rho) \\
&+\frac{9}{2}\mathrm{Re}\left\{\left(\frac{\varepsilon-1}{\varepsilon+2}\right)\cdot\left(\frac{\mu-1}{\mu+2}\right)^*\right\}\cdot I_2(\rho) \ , \\
&Q_{abs}(\rho) = 4\rho\cdot\left|\mathrm{Im}\left\{\frac{\varepsilon-1}{\varepsilon+2}\right\} + \mathrm{Im}\left\{\frac{\mu-1}{\mu+2}\right\}\right| .
\end{aligned}
\tag{2}
$$

Here $I_1(\rho)$ and $I_2(\rho)$ are given by:[6]

$$
\begin{aligned}
&I_1(\rho) = -3 + \frac{\sin 4\rho}{\rho} - \frac{3\left(1-\cos 4\rho\right)}{4\rho^2} + \frac{9\left(1-\cos 4\rho - 8\rho^2\right)}{32\rho^4} + \\
&\quad + \frac{9\left(4\rho - \sin 4\rho\right)}{8\rho^3} + \left(2 - \frac{1}{\rho^2}\right)\cdot I_0(\rho) \ , \\
&I_2(\rho) = -4 + \frac{1-\cos 4\rho}{\rho^2} + \left(2 - \frac{1}{\rho^2}\right)\cdot I_0(\rho) \ , \\
&I_0(\rho) = 2\int_0^{2\rho}\frac{\sin^2 z}{z}dz = C + \ln 4\rho - \mathrm{Ci}(4\rho) \ .
\end{aligned}
\tag{3}
$$

where $C$=0.5772 is the Euler's constant, $Ci(z)$ is the cosine integral.[2]

The analysis of Equations (1)-(3) shows that, depending on the geometrical and optical parameters of a particle and on the light beam parameters, each term in the expression (1) for $F_{ph}$ can be the dominating one. Correspondingly, the dependence of photophoretic force on particle size parameter and optical properties is quite different in these cases. We shall illustrate this by considering a particular, but rather common situation when $\mu$=1 and $\varepsilon'' << |\varepsilon - 1|$. Taking $\Delta\theta > 0$ for divergent beam, $\Delta\theta < 0$ for convergent beam, considering the transverse and the longitudinal gradients of beam irradiance to be $\nabla_\perp(J_0) \approx J_0 / w_0$, $\nabla_\parallel(J_0) \approx -\Delta\theta \cdot J_0 / w_0$, and regarding $(\varepsilon'+2) \approx 3$ because of $|\varepsilon - 1| << 1$, we obtain Eq. 4 from (1)-(3).

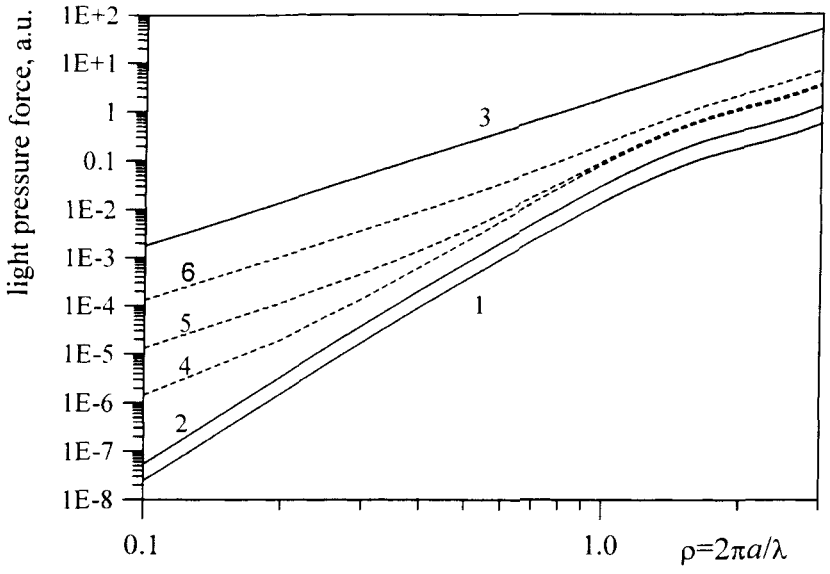


**Figure 1**. Size dependence of the light pressure force, calculated for particles of various materials according to equation (4). 1 - glass ($\varepsilon'$=2.28, $\varepsilon''\approx 0$ at $\lambda_0$=589 nm), 2 - latex ($\varepsilon'$=2.53, $\varepsilon''\approx 0$ at $\lambda_0$=589 nm), 3 - carbon black ($\varepsilon'$=2.4, $\varepsilon''$=2.38 at $\lambda_0$=489 nm), 4-6 - model substances with $\varepsilon'$=1.7 and $\varepsilon''$=0.001 (4), 0.01 (5), 0.1 (6).

$$F_{ph\parallel} \equiv F_{pr} + F_{\nabla\parallel} \approx \varepsilon_m \frac{\lambda^2\rho^2}{4\pi c}\cdot\left[\frac{1}{4}(\varepsilon'-1)^2\cdot I_1(\rho)+\frac{4}{3}\varepsilon''\cdot\rho\right]$$
$$\cdot J_0 - \Delta\theta\cdot F_{\nabla\perp}\ , \qquad (4)$$
$$F_{ph\perp} \equiv F_{\nabla\perp} \approx \varepsilon_m \frac{\lambda^3\rho^3}{12\pi^2 c w_0}\cdot(\varepsilon'-1)\cdot J_0\ .$$

Fig. 1 shows the size dependence of the light pressure calculated for particles with different optical parameters according to relationships (4). For small particles ($\rho<<1$) Equation (3) gives $I_1(\rho)\approx(32/27)\cdot\rho^4$ while, for large particles ($\rho>>1$) $I_1(\rho)\approx 2[\ln(4\rho)+C]-3$. Depending on the relationship between the magnitudes of ($\varepsilon'$-1) and $\varepsilon''$, the non-absorbing, "low absorbing," and "highly absorbing" particles can be distinguished conventionally. For non-absorbing particles with $\varepsilon''=0$ Equation (4) gives $F_{pr} \propto (\varepsilon'-1)^2\cdot\rho^6\cdot J_0$ practically up to $\rho\sim 1$ (Fig. 1, curves 1, 2). For "low absorbing" particles with $\varepsilon''<<(\varepsilon'-1)^2$ it follows from (4) that $F_{pr} \propto \varepsilon''\cdot\rho^3\cdot J_0$ at $\rho<<1$, with the change to $F_{pr} \propto (\varepsilon'-1)^2\cdot\rho^6\cdot J_0$ at higher $\rho$, and possible return to the initial dependence at very large

$\rho$, if the inequality $2\rho|\varepsilon-1| < 1$ still holds at such $\rho$ (Fig. 1, curves 4,5). The transverse gradient force $F_{\nabla_\perp}$ may exceed the radiation pressure for all $\rho<1$ if the beam radius is as small as $w_0<\lambda/|\varepsilon'-1|$, while for the longitudinal gradient force $F_{\nabla_\parallel}$ that requires $w_0<\lambda\cdot\Delta\theta/|\varepsilon'-1|$. The direction of gradient force is determined by the sign of $(\varepsilon'-1)$: the particles with $\varepsilon'>1$ are pulled into the maximum of the radial distribution of field intensity, while the particles with $\varepsilon'<1$ are pushed either out of the beam, or into the minimum of the field intensity. For the "highly absorbing" particles, classified by condition $(\varepsilon'-1)^2<<\varepsilon''<<|\varepsilon'-1|$, the radiation pressure is due to the light absorption mainly, and $F_{pr} \propto \varepsilon''\cdot\rho^3\cdot J_0$. Here $F_{\nabla_\perp}>F_{pr}$ if the beam radius $w_0<\lambda|\varepsilon'-1|/4\pi\varepsilon''$, and $F_{\nabla_\parallel}>F_{pr}$ if $w_0<\lambda\cdot\Delta\theta\ |\varepsilon'-1|/4\pi\varepsilon''$.

The analysis of the direct photophoretic force for Rayleigh-Gans scattering conditions, described by Equations (1)-(4), is expedient for a general insight into the dependence of this force on the particles parameters varied in a broad range. In practice, however, the validity of this approximation is restricted usually by the region of rather small $\rho$ values. For example, in the case of latex particles in water ($n_r$=1.59/1.333 at $\lambda$=589 nm) we have $2\rho|m-1|\approx 0.39\rho$ and, in the case of glass beads ($n_r$=1.51/1.333 at $\lambda$=589 nm), we get $2\rho|m-1|\approx 0.27\rho$. Thus, the range of the quantitative validity of (1)-(4) in these cases is restricted by $\rho<2$-3.

If particle parameters $m(\lambda)$ and $\rho$ fall outside validity limits of analytical approximations considered above, it is necessary to perform the numerical calculations of $Q_{pr}(\rho)$ entering (1) using the exact Mie theory of light scattering by a sphere. Some relevant examples of such calculations can be found in Refs. 2-5, 7, 8. The most detailed and extensive are the results of Ref. 5, where $Q_{pr}(\rho)$ was calculated for the following set of parameters: 1) $n_r$=1.20, 1.33, 1.50 with $\kappa/(n_r-1)$=0, 0.01, 0.1, 1.0, 10, and $\rho$ in the range $0.5\le\rho\le 30$; 2) $n_r$=1.33, $\kappa$=0, $50\le\rho\le 51$ and $100\le\rho\le 102$ with the fine resolution $\Delta\rho$=0.01; 3) $\rho>>1$, $2\rho|m-1|>>1$, $\kappa/(n_r-1)$=0.0001, 0.001, ..., 1.0, 10.

The results of Refs. 2, 3, 5, 7, and 8 can be summarized as follows. For $n_r<1.2$ and $\kappa/(n_r-1)<0.1$ the plot of $Q_{pr}(\rho)$ in the region $0<\rho<30$ is similar to the plot of $I_1(\rho)$ defined by (3), and its behavior agree with the Equations (2)-(4): $Q_{pr}(\rho) \propto \rho^\alpha$, $1<\alpha<4$ (depending on $\kappa$ value) for $\rho<<1$, $Q_{pr}(\rho) \propto \ln(\rho)$ for $\rho>1$, and $Q_{pr}(\rho)\approx$const for $\rho>20$. With the increase of either $n_r$ or $\kappa$, the curve $Q_{pr}(\rho)$ appears to be scaled as a whole to higher values. With the further increase of $n_r$ over $\approx$1.2 and/or $\kappa/(n_r-1)$ over $\approx$1 the dependence $Q_{pr}(\rho)$ at low $\rho$ remains a power law with an increasing amplitude factor, and $Q_{pr}(\rho)$ at large $\rho$ remains a constant, but a maximum starts to develop in the region $1<\rho<10$. The exact position and the amplitude of this maximum depend both on $n_r^{2,8}$ and $\kappa^5$ values.

For non-absorbing spheres ($\kappa$=0) the limiting ($n_r \to \infty$) position of this maximum is $\rho_m$=1.12, and the maximum value is $Q_{pr}(\rho_m)$=2.57 [Ref. 2, Sec. 10.62]. For intermediate $n_r$=1.33-1.8, the position of the maximum obeys an approximate relation $\rho_m \approx 2.5/(n_r-1)$, and the maximum value of $Q_{pr}$ depends rather strongly on the refraction index: $Q_{pr}(\rho_m) \approx 3 \cdot (n_r-1)^{1.362}$ [See Ref. 8]. For absorbing spheres, the development of the maximum in $Q_{pr}(\rho)$ with the increase of $\kappa$ has a similar qualitative picture, and its limiting position for large $\kappa$ is approximately the same as for non-absorbing spheres.[5] The asymptotic value of $Q_{pr}(\rho)$ for $\rho >> 1$ and $2\rho|m-1| >> 1$ varies within $Q_{pr}$=0.956-1.01, depending on $n_r$=1.20-1.75 and $\kappa/(n_r-1)=10^{-4}$-10 [See Ref. 5]. Hence, for such "very large" particles (practically, for $a$>2 μm at $\lambda$~0.5 μm) the light pressure force is described by (1) with $Q_{pr} \approx 1$.

In the case of "geometrically large" particles ($\rho >> 1$ or $a$> ~10 μm for visible range of light) the direct photophoretic force can be calculated also using the geometrical optics approach of reflected and refracted rays, which exert an appropriate light pressure on the particle surface at the refraction points. The total acting force is obtained by integration of this pressure over the particle surface.[9,10] In the framework of this approach, there is no computational difference between the radiation-pressure component and the gradient component of photophoretic force. This approach appears to be most useful for practical design of Photophoretic FFF systems for large particles separation using highly convergent light beams.



## INDIRECT PHOTOPHORETIC MECHANISMS

Indirect photophoretic mechanisms involve, as the primary action of light, a nonuniform heating of particles and/or a surrounding fluid. This heating results in thermophoretic motion of particles due to tangential gradients of interfacial energy arising near the particle surface. Such mechanism of motion can be termed photothermophoresis, to distinguish it from the direct photophoretic mechanisms. Because for real particles neither $n_r$=1, nor $\kappa$=0, the light pressure should always accompany the photothermophoretic force. However, the relative magnitudes and signs of these two contributions to the total phoretic velocity of a particle depend essentially on the optical properties and phase state of particles and surrounding medium. Light pressure always induces the positive photophoresis – away from the light source.

On the contrary, photothermophoresis of solid particles in gaseous ambient may be either positive or negative, depending on the particles parameters and gas pressure.[11] Photothermophoresis of strongly absorbing

liquid drops in another immiscible transparent liquid, according to experiments,[12] is negative, and its magnitude exceeds substantially the contribution from the light pressure.

In regard to photothermophoresis problem, it is natural to consider two mutually complementary extremes: first, a light-absorbing particle surrounded by transparent liquid; second, a transparent particle placed in a channel flow of light-absorbing fluid. Here we shall consider the first extreme only, which can be referred to as the *internal problem*. The other case – the *external problem* – will be considered elsewhere. The solution of photothermophoresis problem includes three rather independent stages: the calculation of the optical field inside and outside the particle; determination of the temperature field resulting from the light absorption; the calculation of the thermophoretic mobility of a particle in this field on the basis of appropriate physicochemical models for the particle, surrounding medium and their interfacial region.



## Optical Problem

The aim of the optical problem is the calculation of the distribution of absorption centers. This distribution is characterized by the source function $B(x,z) = E_i^2(x,z) / E_0^2$, where $E_i(x,z)$ is the electric field strength inside the particle, $E_0$ is the incident plane wave amplitude, $x$ is the radial distance from particle main diameter parallel to the light propagation direction, $z$ is the distance along the main diameter measured from the center of a particle (Fig. 2). Depending on the particle size parameter $\rho$, there are three domains where both the internal field patterns and their calculation procedures are essentially different. If $\rho<<1$ (Rayleigh scattering), the internal field can be considered as a plane wave, exponentially decaying along the main diameter due to absorption. For intermediate $\rho$~1-10, the particle behaves like a spherical cavity, and the internal field distribution is a complicated system of minima and maxima.[13,14] Here $B(x,z)$ strongly depends on particular combination of particle size and optical constants, and can be found only using the rigorous Mie theory.[13,14] In the third domain, $\rho>>10$, a particle behaves like a tiny spherical lens which focuses the incident radiation. The focusing process begins inside the particle, and (for $n_r<2$) is completed in the surrounding medium at some distance from the rear pole of a particle. Here $B(x,z)$ can be successfully calculated using the geometrical optics approach, and the general relationship can be established between the particle parameters and the field distribution. This specific situation, termed the *lens mechanism* of photothermophoresis, will be considered in detail below.

Consider the incident plane wave as a collection of finite pencils of rays parallel to the z-axis, $h$ being the distance of the pencil axis from the z-axis. Each pencil becomes a convergent (for $n_r>1$) or divergent (for $n_r<1$) bundle of rays after the refraction at the particle surface (Fig. 2). Tracing the rays' path inside the particle according to the geometrical optics laws, and taking into account the conservation along the bundle axis of the product of the light intensity and the bundle cross-section,[15-17] we obtain:

a) central bundle, $h$=0:

$$B(z)=\frac{\left[1-R(h)\right]\exp\left[-2\frac{\kappa\rho}{n_0}(z+1)\right]}{\left[1-\frac{n_r-1}{n_r}(z+1)\right]^2}, \qquad z=\frac{\ell}{n_r}-1, \quad n<2 \qquad (5)$$

b) noncentral bundles, $0<h\le 1$:

$$B(x,z)=\frac{h\left[1-R(h)\right]\exp\left[-2\frac{\kappa\rho}{n_0 n_r}\left(\ell-1+\sqrt{1-h^2}\right)\right]}{x(\ell,h)\sqrt{\left(\frac{\partial x}{\partial h}(h,\ell)\right)^2+\left(\frac{\partial z}{\partial h}(h,\ell)\right)^2}},$$

$$x(\ell,h)=h-\left(\ell-1+\sqrt{1-h^2}\right)\frac{\sin(\alpha-\beta)}{n_r}, \qquad (6)$$

$$z(\ell,h)=-\sqrt{1-h^2}+\left(\ell-1+\sqrt{1-h^2}\right)\frac{\cos(\alpha-\beta)}{n_r},$$

$$\alpha=\arcsin(h), \quad \beta=\arcsin\left(\frac{h}{n_r}\right), \qquad \ell\ge 1-\sqrt{1-h^2}, \quad n_r<\sqrt{2}.$$

Here $l$ is the optical path measured from the plane z=-1, i.e., the product of the geometrical distance along the bundle axis and an appropriate refraction index, $R(h)$ is the Fresnel reflection coefficient,[15] $n_0=\sqrt{\varepsilon_m}$. The coordinates and the distances in (5), (6), and below are dimensionless quantities measured in units of particle radius $a$. So, the point (0,-1) corresponds to the front (illuminated) pole of the particle, and the point (0,1) is the rear pole. The relations (5) and (6) are valid until the focal points lie outside the particle, that is for $n_r<2$ for paraxial rays, and $n_r<\sqrt{2}$ for outer rays with $h$=1. They neglect the light reflection inside the particle, for visible range $R<<1$ usually.

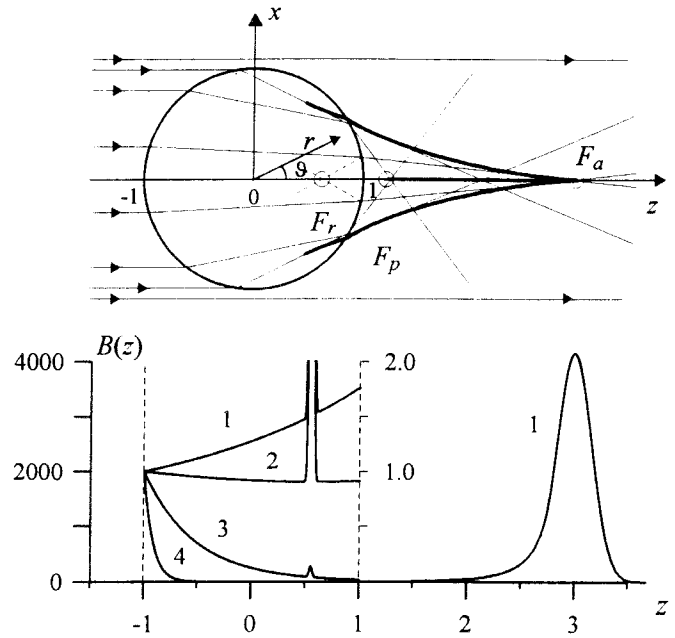


**Figure 2.** Geometrical optics picture of light focusing by a particle (top) and heat sources distribution $B(z)$ along the main optical axis (bottom). Thickened curves are the caustics lines. $F_a$, $F_p$ and $F_r$ are the focal points for paraxial rays, extremely outer rays, and reflected inside the particle rays. Calculations are done for $n_r$=1.2, but picture is qualitatively valid for $1 < n_r < \sqrt{2}$. $B(z)$ curves are calculated for $\kappa\rho$=0.06 (1), 0.23 (2), 1.22 (3), 6.1 (4). Note, that the scales differ by 2000 times inside and outside the particle.

Fig. 2 shows the geometrical optics view of light focusing by a particle, and the distribution of the heat sources along the main optical axis for various values of absorption. Numerical calculations of $B(x,z)$ used for solution of the thermal problem were based on (5), (6) with the inclusion of the first internal reflection of rays. The intensity of the field near the focal points and caustic curves was evaluated using the formulae from Refs. 15-17.

The comparison with the results based on exact Mie theory[14] showed, that the geometrical optics approach gives good quantitative results starting from $\rho > 10^2 \div 10^3$ (depending on specific values of $n_r$ and $\kappa$), while the qualitative agreement keeps down to $\rho \sim 10$.

**Thermal Problem**

The temperature distribution $T(r,\theta)$ is defined by the stationary heat-transfer equation with the heat sources proportional to the source function $B(r,\theta)$:[13,14]

$$\nabla^2 T(r,\theta) = -\frac{4\pi n_r \kappa}{\lambda_0 k_i} I_0 B(r,\theta) \tag{7}$$

where $k_i$ is the thermal conductivity of the particle. Due to the axial symmetry of the problem the polar coordinates are used, the polar angle $\theta$ being measured from the rear pole (Fig. 2). It is expedient to introduce the characteristic temperature $T_0$ of particle's heating due to the light absorption and to use the dimensionless temperature $\tau(r,\theta)=T(r,\theta)/T_0$. Then, the thermal problem can be written as:

$$\begin{aligned}
&\nabla^2 \tau_i(r,\theta) = -B(r,\theta), && |\vec{r}| \le 1 \\
&\nabla^2 \tau_e(r,\theta) = 0, && |\vec{r}| > 1 \\
&\tau_i = \tau_e, \quad k_i \vec{\nabla} \tau_i = k_e \vec{\nabla} \tau_e, && |\vec{r}| = 1 \\
&\tau_e = \tau_\infty, && |\vec{r}| = R_0 \\
&T_0 = 2\kappa\rho \frac{n_r a}{n_0 k_i} I_0, \qquad \rho = \frac{2\pi a n_0}{\lambda_0}.
\end{aligned} \tag{8}$$

Here, indexes i and *e* refer to the particle and to surrounding medium, $k_e$ is the thermal conductivity of the medium, $T_0 \cdot \tau_\infty$ is the ambient temperature far from the particle, $R_0 >> 1$ is a characteristic outer boundary of the temperature field induced. In our calculations we took $R_0=100$.

As Equations 5 and 6 show, the source function $B(r,\theta)$ depends on two parameters of the particle, $n_r$ and $\kappa\rho$. Hence, the solution $\tau(r,\theta)$ of (8) depends on three parameters: $n_r$, $\kappa\rho$, and $(k_i/k_e)$, the latter having rather small influence in practically important range of values. Thus, the use of dimensionless temperature in units $T_0$ enables to obtain a general-type solution, which can be used both for general analysis of photothermophoresis phenomenon and for numerical evaluation of particular cases.

The main interest presents the temperature distribution over the particle surface. As Fig. 3 shows, three essentially different distribution types may exist depending on the combination of the size and optical constants of a particle,

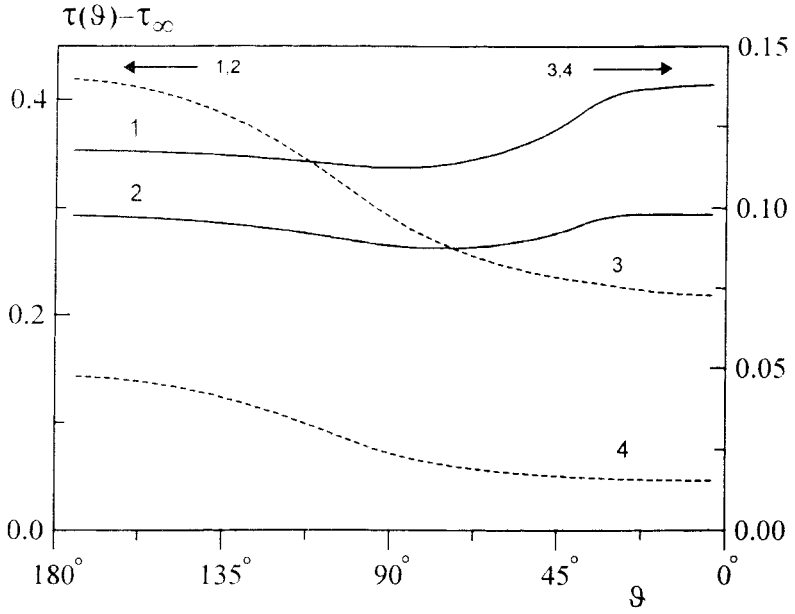


**Figure 3**. Surface temperature distributions calculated for a light-absorbing particle. $k_i=k_e$ ; $n_r=1.2$, $\kappa\rho=0.06$ (1), 0.23 (2), 1.22 (3), 6.1 (4).



mainly, on the $\kappa\rho$ value. They correspond to the three main types of *B(z)* curves shown at Fig. 2. If $\kappa\rho<<1$, the rear pole domain of a particle is heated preferentially due to the light focusing (see curve 1 for *B(z)* in Fig. 2 and curve 1 in Fig. 3). With the increase of $\kappa\rho$, the attenuation of light due to the absorption in the particle material becomes significant enough to compensate the focusing effect (curve 2 for *B(z)* at Fig. 2). So, for some intermediate $\kappa\rho$=0.13-0.34 (depending on the $n_r$=1.1-1.4) the poles temperatures became equal, while the temperature minimum with the depth of 6-8% develops near the equatorial strip $\theta\sim90^0$ (curve 2 in Fig. 3). For high absorption values ($\kappa\rho$>0.5-1), the attenuation of light prevails over the focusing, so the front pole has the highest temperature value, which decreases monotonously along the surface to the rear pole (curves 3, 4). Fig. 4 shows the dependencies of poles temperatures on the "optical density" $\kappa\rho$ of a particle. They were calculated in the general form using (8), and then were specified by multiplication by $T_0$ to a particle of diameter $2a$=50 μm and to some particular value $I_0=10^7$ W/m$^2$ of laser power density. This value corresponds to 1 W of $Ar^+$-ion laser radiation focused into the spot of $\sim2\cdot10^{-4}$ m diameter. These plots can be easily scaled to any other values of $I_0$ and a using the formula (8) for $T_0$.

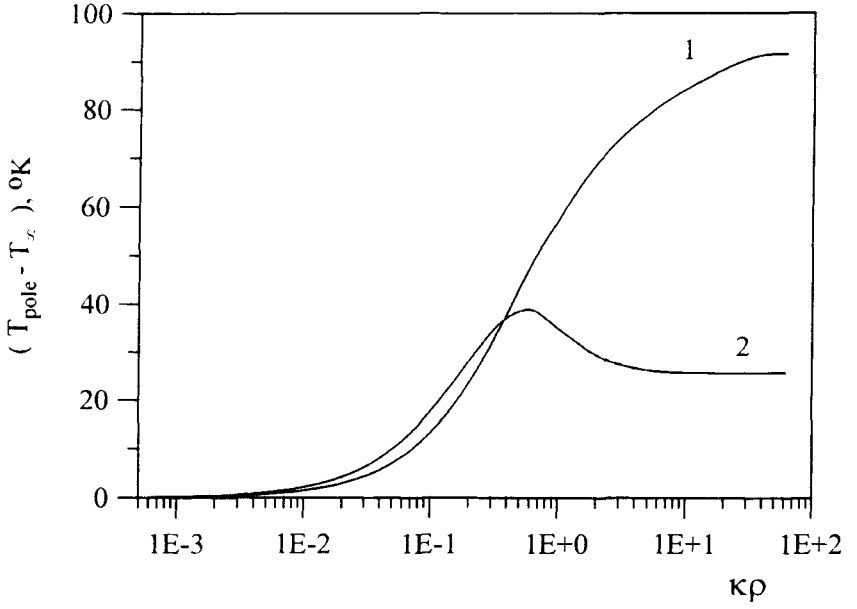


**Figure 4**. Temperature of the front (1) and the rear (2) poles of light-absorbing particle as a function of the absorption parameter κρ, calculated for $I_0=10^7$ W/m$^2$, λ=514 nm, $a=5\cdot10^{-5}$ m (ρ=406), $k_i=k_e=1$ W/m/$^0$K, and $n_r=1.4$.



## Photothermophoretic Mobility

With the known temperature distribution, the problem reduces to the calculation of particle thermophoretic mobility for the given temperature field. We consider a solid particle in electrolyte solution, using the approach suggested initially in Ref. 18 and further developed in Refs. 19-21.

According to this approach, phoretic motion of a particle arises due to the flow generated within the thin interfacial region near its surface by the interaction between the ion (molecular) solute and some external (electrical, thermal etc.) applied field. A specific distinctive feature of photothermophoresis is that this "external" temperature field arises from the particle's heating by light. Because characteristic width of interfacial layer is usually small compared with the particle size, this layer can be considered as locally flat. So, the flow velocity profile is defined by two-dimensional Stokes equations:[18-20]

$$\frac{\eta}{a}\frac{\partial^2 u}{\partial \xi^2}-\frac{\partial p}{\partial \zeta}=0\,,\quad \frac{\partial p}{\partial \xi}+C_m(\xi)\frac{\partial \Phi}{\partial \xi}=0$$
$$u\big|_{\xi=0}=0\,,\quad \left.\frac{\partial u}{\partial \xi}\right|_{\xi\to\infty}=0\,,\quad p\big|_{\xi\to\infty}=p_0\,. \tag{9}$$

Here $\xi$ is the normal and $\zeta$ is the tangential dimensionless coordinates at some point $(r,\theta)$ at the particle surface, $\Phi(\xi)$ is the interaction potential of solute ions with the surface, $C_m(\xi)$ is the ions concentration distribution near the surface, $\eta$ is the fluid viscosity, $u(\xi)$ is the fluid velocity field near the surface, $p(\xi,\zeta)$ is the pressure field. The directions of $\zeta$-axis and z-axis coincide for $\theta=90^0$. The ions concentration near the surface obeys the Boltzmann distribution law: $C_m(\xi)=C_{m0}\cdot\exp[-\Phi(\xi)/k_BT]$, where $C_{m0}$ is the bulk ions concentration, $k_BT$ is the thermal energy. The use of this expression for $C_m(\xi)$ in the second Equation 9 gives, after the direct integration, the pressure field in the interfacial layer $p(\xi,\zeta)$. Due to the gradient of the surface temperature, this pressure has the tangential gradient which induces the fluid flow along the particle surface. The flow velocity is obtained from the second of Equations 9 after substitution of $p(\xi,\zeta)$ and integration by parts with the use of the boundary conditions (Eq. 9). Taking into account that in dimensionless form $\xi=r-1$ and $d\zeta=-d\theta$, we get for $u(\xi,\theta)$ and for the slip velocity $u^S=u(\xi\to\infty)$ at the outer boundary of interfacial layer:

$$u(\xi,\theta)=C_{m0}k_BT_0a\left\{\int_\xi^\infty \xi\frac{\partial\tau(1+\xi,\theta)}{\partial\theta}W(\xi,\theta)d\xi+\int_0^\xi \xi\frac{\partial\tau(1+\xi,\theta)}{\partial\theta}W(\xi,\theta)d\xi\right\}$$
$$u^s=C_{m0}k_BT_0a\int_0^\infty \xi\frac{\partial\tau(1+\xi,\theta)}{\partial\theta}W(\xi,\theta)d\xi\,,$$
$$W(\xi,\theta)=\frac{1}{\eta}\left\{\exp\left[-\frac{\Phi(\xi,\theta)}{k_BT_0\tau(1+\xi,\theta)}\right]\cdot\left[1+\frac{\Phi(\xi,\theta)}{k_BT_0\tau(1+\xi,\theta)}\right]-1\right\}. \tag{10}$$

The local temperature $T_0\cdot\tau(r,\theta)$ in (10) is the solution of the thermal problem (Eq. 8). The use of (10) and the general hydrodynamic result[20]

$$\vec{u}_{ph}=-\frac{1}{S}\oiint_S \vec{u}^s dS \tag{11}$$

enables to determine the resulting particle velocity $\vec{u}_{ph}$. The integration in (11) is done over the outer boundary of the interfacial layer, i.e., practically over the particle surface.

To keep the connection with the usual thermophoresis, it is convenient to define the magnitude of photothermophoretic mobility $b_{phth}$ of a particle from the relation $u_{ph}=b_{phth}\cdot(T_0/a)$. Here $T_0/a$ is the characteristic temperature gradient of the problem, which is proportional to the incident light intensity $I_0$ (see (8)). The sign of $b_{phth}$ is taken, usually, as positive when the directions of $\vec{u}_{ph}$ and $\vec{I}_0$ coincide. Taking into account the axial symmetry of the problem and the relations $u_x^s = u^s\cdot\cos\theta$, $u_y^s = u^s\cdot\sin\theta$, we get from (10), (11):

$$b_{phth} = -\frac{k_B C_{m0} a^2}{2}\int_0^{\pi}\int_0^{\infty}\xi\frac{\partial\tau(1+\xi,\theta)}{\partial\theta}W(\xi,\theta)\sin^2\theta\,d\xi\,d\theta \qquad (12)$$

The formula (12) can be further simplified considering that, in practice, $\tau-\tau_\infty \ll \tau_\infty$, and variations of the temperature with $\xi$ and $\theta$ near the particle surface are mutually independent:

$$\tau(1+\xi,\theta) \approx \tau_\infty + f_1(\xi)\cdot f_2(\theta) \qquad (13)$$

As the numerical calculations showed, in the range $1<1+\xi<1.2$ the relationship (13) holds true with the accuracy better then 1% for all $\theta$. Note that, for a particle in a constant external temperature gradient $\vec{\nabla}T$ the relationship (13) is the exact result: $T = T_0 + \nabla T\cdot r\cdot\cos\theta$. From (12) and (13) we obtain finally:

$$u_{ph} = b_{phth}\cdot\frac{T_0}{a}, \qquad b_{phth} = b_{th}\cdot g_{an}(n_r,\kappa\rho), \qquad \frac{T_0}{a} = 2\kappa\rho\frac{n_r I_0}{n_0 k_i},$$

$$b_{th} = \frac{2k_B C_{m0} a^2}{2+\frac{k_i}{k_e}}\int_0^{\infty}\xi W(\xi,\theta) f_1(\xi)\,d\xi,$$

$$g_{an}(n_r,\kappa\rho) = -\frac{1}{4}\left(2+\frac{k_i}{k_e}\right)\int_0^{\pi}\frac{d\tau(1,\theta)}{d\theta}\sin^2\theta\,d\theta. \qquad (14)$$

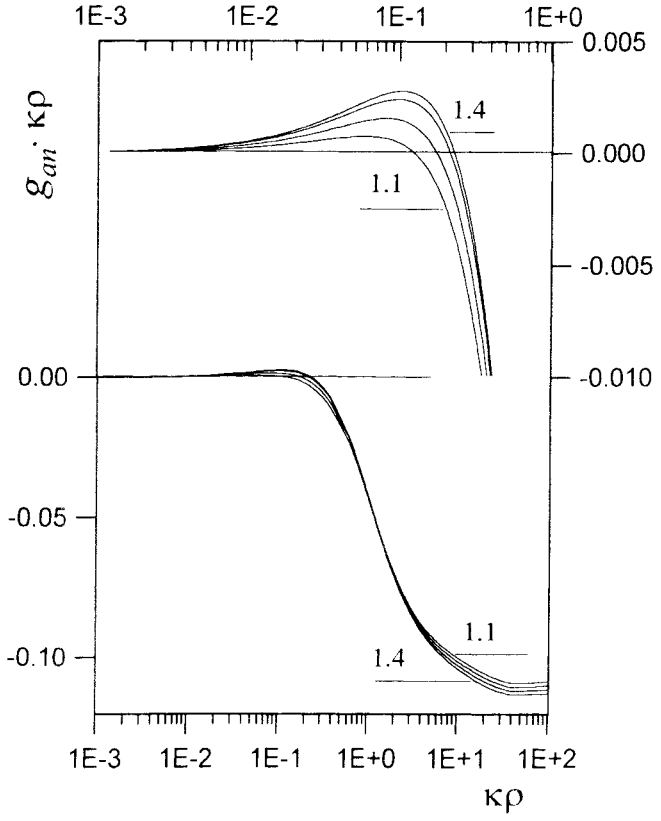


**Figure 5**. Dependence of the optical heating factor $g_{an}(n_r, \rho)\cdot\kappa\rho$ of photothermophoretic velocity of a particle on its size and optical constants. Curves are calculated for increasing values of $n_r$=1.1, 1.2, 1.3, 1.4, and for $k_i=k_e$ . It is supposed that $\rho>10$.

According to (14), the photothermophoretic mobility of a particle is a product of its ordinary thermophoretic mobility and the factor $g_{an}(n_r,\kappa\rho)$. The latter is actually the surface average of the dimensionless gradient of the surface temperature of a particle. For $\kappa\rho<<1$, when the focusing process governs the internal distribution of light intensity, $[d\tau(1,0)/d\theta]<0$ (see Fig. 3), hence, $g_{an}(n_r, \kappa\rho)>0$. For $\kappa\rho>1$, when the main governing factor is the light absorption, $[d\tau(1,0)/d\theta]>0$ and $g_{an}(n_r, \kappa\rho)<0$. Fig. 5 shows the plots of the product $\kappa\rho\cdot g_{an}(n_r, \kappa\rho)$, which determines the dependence of photothermophoretic velocity of a particle on its optical constants and size.

The thermophoretic mobility of solid particle in electrolyte solution was considered.[21] For the model of electrostatic attractive potential at the particle surface, the result has the form:

$$b_{th} \approx -\frac{2k_B C_{m0}\delta^2(W_0-3)\exp(W_0)}{\eta\left(2+\frac{k_i}{k_e}\right)W_0^2}; \qquad \delta^2 \approx \frac{\varepsilon_0\varepsilon_m k_B T}{2C_{m0}(Ze)^2} \quad (15)$$

Here $W_0$ is the depth of potential well in units of thermal energy $k_BT$, $\delta$ is the width of the double electric layer near the particle surface, Ze is the charge of ions in electrolyte, $\varepsilon_m$ is the relative dielectric constant of the liquid, $\varepsilon_0$ is the absolute permittivity. Formula (15) was derived for $W_0$ exceeding ~5, so for solid particles in electrolytes $b_{th}<0$. Hence, we obtain that photothermophoretic mobility of such particles is negative for $\kappa\rho<<1$, goes through the zero in the range $\kappa\rho\sim0.1\div0.3$, then stays positive and monotonically increases for $\kappa\rho>0.5$, with the saturation at very high $\kappa\rho$ values ~40.

Consider the relative magnitudes of the contributions from the light pressure and photothermophoresis to the total velocity of a particle. Using (1), (14), (15), we obtain:

$$\frac{u_{ph}}{u_{pr}} = -48\pi c k_B \frac{\kappa\rho\cdot g_{an}(n_r,\kappa\rho)}{\rho\cdot Q_{pr}(n_r,\kappa\rho)}\cdot\frac{n_r C_{m0}\delta^2(W_0-3)}{\lambda_0 k_i\left(2+\frac{k_i}{k_e}\right)W_0^2}\exp(W_0) \quad (16)$$

For typical values $W_0=5$, $n_r=1.2$ at $\lambda_0=500$ nm, and $k_i\approx k_e=1$ W/m/$^0$K that gives $(u_{ph}/u_{pr})= -1.13(\kappa\rho\cdot g_{an}/\rho Q_{pr})T(^0K)$. Using the plot of $\kappa\rho\cdot g_{an}$ from Fig. 5 and $Q_{pr}\approx0.35$,[5,7,8] the estimate for a particle with $2a=5\cdot10^{-5}$ m ($\rho$=418) at $\kappa\approx0.1$ and $T\approx300$ K is $(u_{ph}/u_{pr})\approx0.5$. Hence, for large absorbing particles, the photothermophoretic velocity component can be quite comparable with the light pressure component.

## EXPERIMENTAL

The observations of particles photophoresis were made in two experimental arrangements. First, the motion of solid particles under the action of green light ($\lambda$=514.5 nm) from the Coherent INNOVA'300 $Ar^+$-ion laser was observed using the microscope. The laser beam was focused by a lens with the focal distance 10 cm at the opening of a glass capillary with a

**Table 1**

**Characteristic Photophoretic Velocities of Various Particles***

| Type and Diameter of Particles | Mean Velocity, μm/sec | Maximum Velocity Observed, μm/sec |
|---|---|---|
| latex red, 3 μm | 7.4±2.3 | 10.3 |
| latex white, 20.5 μm | 13.5±1.7 | 15.7 |
| latex red, 20.1 μm | 24.3±2.5 | 26.3 |
| glass, 22.1 μm | 34.5±3.9 | 38.5 |

*Measured at P=0.36 W ($J_0 \approx 7.2 \cdot 10^7$ W/m$^2$ ).



**Table 2**

**Characteristic Values of Photophoretic Velocities Measured for Glass Beads of 22.1μm Diameter at Various Magnitudes of Laser Power**

| Incident Light Irradiance, W/m$^2$ | Mean Velocity, μm/sec | Maximum Velocity Observed, μm/sec |
|---|---|---|
| $7.2 \cdot 10^7$ | 34.5±3.9 | 38.5 |
| $9.0 \cdot 10^7$ | 53.6 | 53.6 |
| $10.7 \cdot 10^7$ | 64.4±35.6 | 130.4 |

rectangular cross-section, placed horizontally at the microscope stage along the beam direction. The capillary of ~300 μm height, ~5 mm breadth and 4 cm length was filled with a suspension of particles in distilled water. Particles velocity was evaluated using the eyepieces' graticules and the stop clock. The particles investigated were monodisperse white and red latex spheres, glass microspheres, and carbon black particles taken from polydisperse mixture subjected to sonication. The laser power P varied from 0.1 to 0.8 W. The diameter of focused laser beam was evaluated from the light-scattering trace visible in the suspension to be ~80 μm. That gave a relation $J_0 \approx 2 \cdot 10^8 \cdot P(W)$ W/m$^2$ for the mean incident light irradiance.

The results of direct velocity measurements are given in Tables 1,2. The positive photophoresis was observed for all particles. Within the measurements' uncertainty, their photophoretic velocity depended linearly on

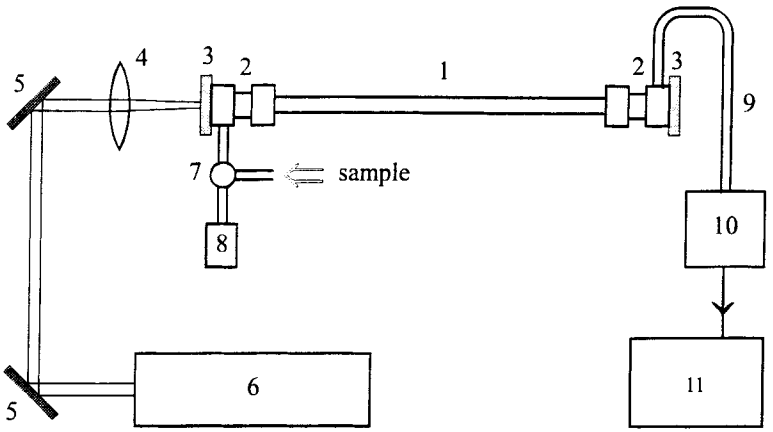


**Figure 6**. Experimental arrangement used for registration of particles photophoresis in a flow: 1 -metallic capillary; 2 - standard metallic gasket with a specially machined and polished face; 3 - optical window (glass plate) glued to the gasket; 4 - lens; 5 - mirror; 6 - $Ar^+$-ion laser; 7 - injection valve; 8 - syringe pump; 9 - output tubing; 10 - UV-detector; 11 -chart recorder.



the incident light irradiance. For carbon black particles of ~12 μm diameter and for latex particles of 9.87 μm diameter, the best-fit lines were y=4.77x+0.51 (carbon black) and y=1.08x-0.24 (latex) in the range 0<x<7, where y is $u_{ph}$ in μm/sec, x is $J_0$ in $10^7$ W/m$^2$.

In the second arrangement, shown at Fig. 6, the observations were made of the redistribution of polydisperse carbon black particles in a flow under the action of laser light. The laser beam was focused at the entrance window of a round channel in the direction of suspension flow. To prevent the light escape from the channel due to the refraction, the channel was made of a metallic capillary. It had 0.765 mm inner diameter and 168 mm length. The elution curves of polydisperse carbon black particles injected into a flow of distilled water were registered using a UV detector in the gravity-sedimentation FFF conditions with the laser power switched on and off. The flow velocity at the channel axis was estimated to be 1.2 mm/sec. Typical elution curves are shown in Fig. 7. They had a strong initial maximum which we believe to correspond to the small particles fractions, and a considerably lower secondary maximum which can be attributed to larger particles. (No special measurements with the calibrated particles were carried out to determine exactly the operation mode of the channel system used).

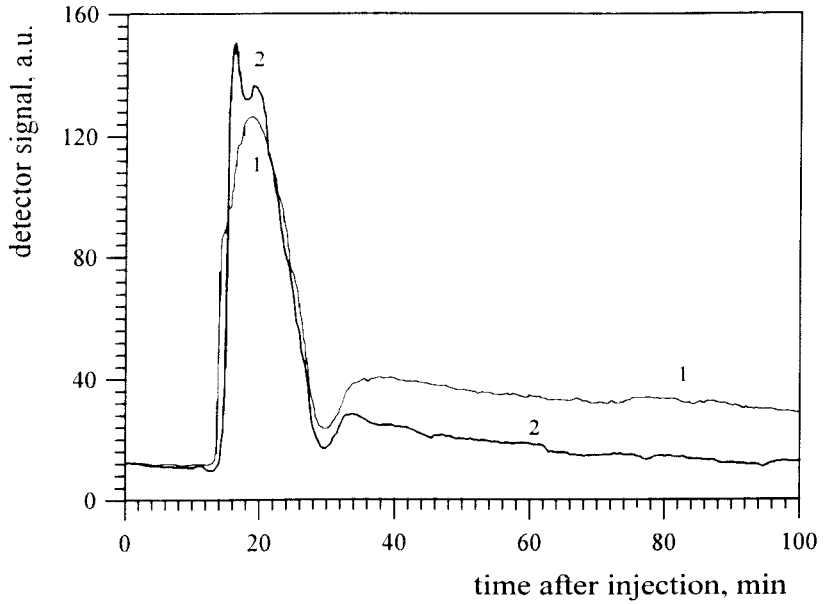


**Figure 7**. Elution curves obtained for injected samples of polydisperse carbon black particles using the flow system shown at Fig. 6: (1) - with no light; (2) - under the action of the focused laser light of 0.65 W power at $\lambda$=514.5 nm.



As Fig. 7 shows, the laser light action manifested itself as a change in the shape (splitting) of the initial maximum, and as a 4-5 minutes (~11%) shift of the secondary maximum towards the smaller times. The latter shift evidences the acceleration of particles along the flow under the light action.

## DISCUSSION

Both the direct observations and the shape changes of the elution curves evidence the positive photophoresis of large solid particles in a fluid, namely, the motion in the direction of light propagation. The microscopic observation showed no visible indications, such as gaseous bubbles or convection flows, of appreciable heating of particles or surrounding water, even in the case of carbon black particles, provided the suspension was dilute enough. The estimates of the temperature rise due to the light absorption also give negligibly small values both for water and for latex or glass particles. Thus, the primary mechanism of the motion observed seems to be the light pressure, at least for

latex particles and glass beads. However, the contribution from the photothermophoretic mechanisms can be large enough in the case of highly absorbing carbon black particles. Let us estimate photophoretic velocities of particles under the observation conditions using the theoretical results of preceding sections. In water, the latex particles have $m_{rel}$=1.191 at $\lambda_0$=589 nm, and carbon black particles have $m_{rel}$=1.27-i·0.52 at $\lambda_0$=489 nm. The particles investigated had very large values of size parameter, ranging from $\rho$=24.45 for $2a$=3 mm up to $\rho$=180.2 for 2a=22.1 μm. According to Mie theory,[2,5,8] for such $\rho$ values the efficiency factor $Q_{pr}(\rho)\approx$const, the estimates being $Q_{pr}\approx$ 0.25 for latex and glass particles, and $Q_{pr}\approx$1.1 for carbon black particles. From the formula (1) we obtain $u_{ph}\approx 7\cdot 10^{-7}\cdot J_0(W/m^2)$ μm/sec for latex particles and $u_{ph}\approx 3\cdot 10^{-6}\cdot J_0(W/m^2)$ μm/sec for carbon black particles of size $2a\approx$10 mm in water. For carbon black particles, the formula (16) gives also $(u_{ph}/u_{pr})\approx$0.4 at T=300 °K. These estimates agree with slopes ratio $u_{carb}/u_{lat}$=4.4 of the best-fit lines for the measured light intensity dependencies of photophoretic velocities of latex and carbon black particles. The absolute values of the measured velocities are systematically lower than the estimated values, but this seems to be a result of overestimation of the incident laser power in the process of microscopic observation. It should be noted also that, for the same laser power the magnitudes of particles, velocities registered under the microscopic observations will be substantially higher then those observed in the channel measurements, because of light divergence in the channel.



Both the experimental observations and the theoretical estimates of the light-induced velocities of particles show, that velocities in the range 10-100 μm/sec (depending on the particles material and light intensity) can be easily obtained under FFF conditions using the focused laser radiation. These values can even be comparable with some flow velocities used in FFF, as evidences the change of the elution curves of Fig. 7 registered in the longitudinal field-flow geometry. In practical schemes of Photophoretic FFF, the incident light irradiance will be considerably lower because in the transverse field-flow geometry it is rather difficult to produce such a high irradiance value along the whole surface of a channel wall. So, the photophoretic velocities expected for the practical schemes will be essentially lower then those reported in this work. However, the transverse velocities of particles required for their longitudinal separation are also very small compared with the flow velocity. That gives a reason to expect, that the practical transverse-geometry Photophoretic FFF schemes can be implemented. The most promising is the use of highly convergent light beams enabling the light-trapping of particles[9,10] due to the gradient force, and the use of photophoretic forces in combination with some counter-balancing force, such as the gravity force.

## ACKNOWLEDGMENTS

This work was supported, in part, by the RFBR grant #95-03-08390-a.

## REFERENCES

1. J. C. Giddings, Chem. Eng. News, **66**, 34-45 (1988).

2. H. C. van de Hulst, **Light Scattering by Small Particles**, Wiley, New York, 1957.

3. M. Kerker, **The Scattering of Light and Other Electromagnetic Radiation**, Academic Press, New York, 1969.

4. C. F. Bohren, D. R. Huffman, **Absorption and Scattering of Light by Small Particles**, Interscience, New York, 1983.

5. W. M. Irvine, J. Opt. Soc. Am., **55**, 16-21 (1965).

6. A. V. Kats, Izvestija VUZov. Radiofizika, **18**, 566-576 (1975). [in Russian].

7. K. S. Shifrin, I. L. Zelmanovich, Optika i Spectroscopija, **17**, 113-118 (1964). [English Translation: Optics and Spectroscopy (USSR), **17**, 57 (1964)].

8. K. S. Shifrin, Optika i Spectroscopija, **18**, 690-697 (1965). [English Translation: Optics and Spectroscopy (USSR), **18**, 1345 (1965)].

9. G. Roosen, Canad. J. Phys., **57**, 1260-1279 (1979).

10. A. Ashkin, Biophysical J., **61**, 569-582 (1992).

11. M. Kerker, D. D. Cooke, J. Opt. Soc. Am., **72**, 1267-1272 (1982).

12. A. T. Sukhodol'skii, Bull. Acad. Sci., USSR, Physical Series, **50**, 51-57 (1986). Translated and published by Allerton Press, New York.

13. P. W. Dusel, M. Kerker, D. D. Cooke, J. Opt. Soc. Am., **61**, 55-59 (1979).

14. A. P. Prishivalko, **Optical and Thermal Fields Inside Light-Scattering Particles**, Nauka i Tekhnika Publ., Minsk, 1983. [in Russian].

15. M. Born, E. Wolf, **Principles of Optics**, Pergamon Press, Oxford, London, Edinburgh, New York, Paris, Frankfurt, 1964.

16. S. Solimeno, B. Crosignani, P. DiPorto, **Guiding, Diffraction, and Confinement of Optical Radiation**, Academic Press, Orlando, etc, 1986.

17. Yu. A. Kravtsov, Yu. I. Orlov, **Geometrical Optics of Nonhomogeneous Media**, Nauka Publ., 1980. [in Russian].

18. B. V. Derjaguin, G. P. Sidorenkov, E. A. Zubaschenko, E. P. Kiseleva, Kolloid. Zh., **9**, 335-341 (1947). [in Russian].

19. V. G. Levich, **Physicochemical Hydrodynamics**, Prentice-Hall, Englewood Cliffs, New Jersey, 1962.

20. J. L. Anderson, Ann. Rev. Fluid Mech., **21**, 61-99 (1989).

21. J. C. Giddings, P. M. Shiundu, S. N. Semenov, J. Colloid Interfacial Sci., **176**, 454-458 (1995).

Received February 4, 1997
Accepted April 17, 1997
Manuscript 4454